Engineering Structures 285 (2023) 115997

Contents lists available at ScienceDirect

Engineering Structures

journal homepage: www.elsevier.com/locate/engstruct

Advanced numerical insights for an effective seismic assessment of historical masonry aggregates

Mattia Schiavoni [a], Ersilia Giordano [a], Francesca Roscini [b], Francesco Clementi [a,*]

[a] Department of ICEA, Università Politecnica delle Marche, Via Brecce Bianche 12, 60131 Ancona, Italy
[b] Niccolò Cusano University, Via Don Carlo Gnocchi 3, 00166 Rome, Italy

ARTICLE INFO

Keywords:
Masonry
Finite Element Method
Discrete Element Method
Non-Smooth Contact Dynamic Method
Concrete Damage Plasticity
Non-linear dynamic analysis

ABSTRACT

The structural assessment of ancient masonry structures is still a challenging task. The main reasons have been related to the shortage of information in the materials' characterization along with the complex geometry and different evolutions of its constituents' parts through the time. Scientific studies on the evaluation of the structural capacity and design of these masonry buildings have reported several modelling techniques. The goal of this work is to investigate the effectiveness of different numerical approaches in the simulation of the cyclic behaviour of historic masonry buildings under seismic loads. In addition, the damage level of the structural interconnections will be evaluated and what extent they affect the global instability. The specific case study seeks to examine an ancient palace with its civic tower hit by the 2016 Central Italy earthquake. A couple of masonry modelling are used: the first one is discontinuous (DM) and the second one is continuous (CM). Two models were set: one model replicated the structure as a whole, the other one considered only the tower. The DMs were studied with 3DEC© and LMGC90© software, where, in turn, different contact conditions were implemented. In parallel, the CMs were analysed with the Midas FEA NX©. The present research offers significant outcomes obtained from the non-linear dynamic analyses performed using the proper sequence recorded in that seismic event. Likewise, this document underlines the importance of the correct modelling techniques definition, based on the state of the case study, especially when an isolated tower is considered.

1. Introduction

Over the years heritage masonry constructions have demonstrated their extreme brittleness to horizontal loads such as earthquakes. The damages observed after the recent seismic sequences recorded in central Italy between 2016 and 2017 have highlighted the extreme vulnerability of these historical structures [1–4], owing to their irregular geometry [5,6], uneven evolutions across time [7,8], and the inadequate conservation status [9]. These structures have usually shown as aggregates wherein they are characterized in the assembling of different buildings, each other interacting [10–14]. As also confirmed by some authors, the reliability of these structural connections could be correctly evaluated considering their influence on the structural response [15–18].

In the common practice, for the box-like behavior, an appropriate procedure was proposed to verify the assessment of these ancient constructions [19], in which the vertical masonry panels make up the piers and the bands between the openings make up the spandrels. Moreover, their intersection points are considered with rigid links. However, this simplification could be employed for restricted heritage structures characterized by regular geometry, equal floor levels, windows' alignments, etc.

The process to find the best implement possible to simulate such types of constructions has started many years ago and is still ongoing [20,21]. The block-based and the continuous homogenization are the main models that have been receiving the greatest attention.

In the first one, the masonry response is simulated by considering the distinct roles played by the blocks and the mortar. Detailed and simplified micro modellings are included in this process. Both blocks and mortar are represented in the detailed approach [22,23]: differently in the simplified one, the mortar thickness is fully-embodied within the blocks' geometry [24,25]. This modelling can be set both through Finite Element (FE) and Distinct Element (DE) codes. In FE, the masonry is idealized as a continuous medium where the units are connected, at least, to interface elements [26]. In DE, the masonry response is attributed principally to the interactions between blocks with appropriate contact laws obtained starting from the mechanical characteristics of

* Corresponding author.
E-mail address: francesco.clementi@univpm.it (F. Clementi).

https://doi.org/10.1016/j.engstruct.2023.115997

Available online 2 April 2023

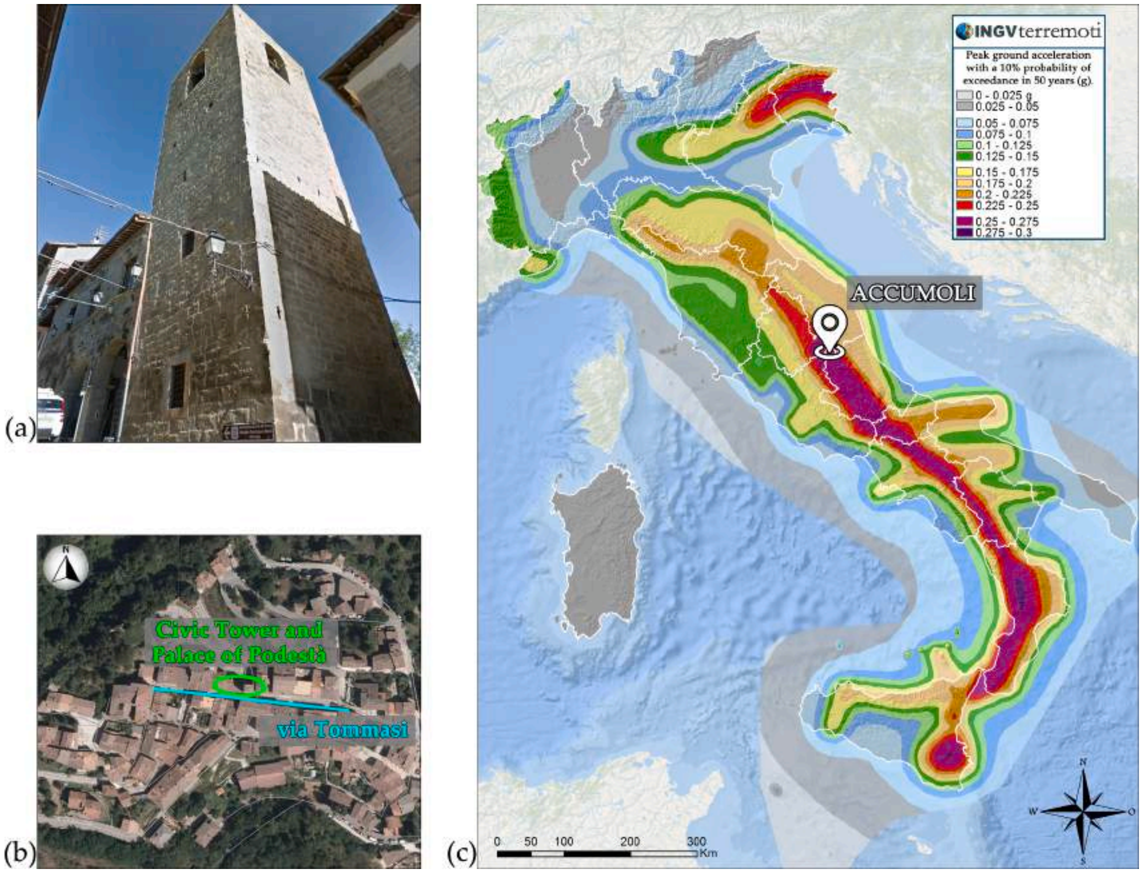

Fig. 1. Case study's photo(a); localization of the case study in the historical center of the village(b); localization of Accumoli in the Italy seismic territory (c).

both mortar and bricks. Finally, in some studies, it is possible to find a combination of DE and FE [27,28].

Conversely, the continuous model makes no distinction between the masonry constituent elements. Indeed, each masonry member is simplified by means of this method as a continuous deformable body. In addition, its final real response is also dependent on the application of appropriate constitutive laws that will help the simulation, with rather adequate approximation [29–32]. Typically, an elastic plastic damage constitutive law simulating the local loss of masonry material strength in the non-linear range is used [33]. The intrinsic constitutive relations can be either directly drawn from calibration through standard experimental tests [34] or indirectly obtained from similar masonry reference studies available in the literature [35]. Compared to the block-based one, less time is required for the modelling process and the analysis execution.

Therefore, from these papers, it comes to light that in the DE model the blocks can move with geometric nonlinearities until the collapse. This makes the DE especially suitable for the investigation of the out-of-plane mechanisms and, if appropriately discretized, even crumbling that frequently characterize the behavior of masonry walls of historic structures under strong interaction between horizontal and vertical dynamic loads. On the other hand, the assumptions of the continuous modelling are based on the full connections between the walls. It mainly allows for the detailed observation of the in-plane structural response. Even if, in this case, the cracks' formation may help to identify the walls most prone to the out-of-plane mechanisms.

The primary objective of this study is to assess what extent the global buildings' response during an earthquake is affected by the singular structural units, one another interacting in each aggregate. To reach this purpose, the case study of the Podestà Palace with its civic tower was considered. This cultural building is located in Accumoli, a small village in the Lazio Region (Fig. 1). As reported in Fig. 1.c, Accumoli is within one of the Italian areas with the highest seismic accelerations. Indeed, this village was severely devastated by the seismic sequence that occurred between 2016 and 2017. To date, the case study is the only palace of the historical center still standing.

Aiming at investigating the structural interactions, two different geometrical models are designed: the first one for the entire structure and the second one just for the tower. These are implemented by simulating the masonry as both a 3D block assembly and a continuous homogeneous material (**Section 4**). For the first, the non-linearity is assigned using laws characterized by both the smooth (**Section 4.1**) and the non-smooth (**Section 4.2**) contacts, and carried out for the analyses in the software LMGC90© and 3DEC©, respectively. Conversely, in the continuous approach, the Concrete Damage Plasticity (CDP) is employed in Midas FEA NX© (**Section 4.3**). The responses of the models are examined through non-linear dynamic analyses, which are performed by applying the main seismic accelerations registered nearby the case study in 2016 (**Section 4.4**). Finally, the numerical results are displayed in terms of damages and time-history shifts (**Section 5**).

2. Historical developments and geometric configuration

From the very few historical information available about the building, this palace seems to be the oldest in Accumoli. There has been the first evidence in dating its existence to the XII Century when the village was under the kings of Naples' domain. The square plan of the tower and the two arched windows of the entrance suggest that its first destination was a public building.

Regarding the complex's geometric arrangement, three buildings are identified: the civic tower on the south-east, the main structure known as the Podestà Palace on the south, and an annex on the north (Fig. 2).

The horizontal square section of the tower is 6.15 m on each side, with 20.00 m of maximum height. The walls' thickness is almost constant and equal to 1.20 m. It shows four single-arch windows

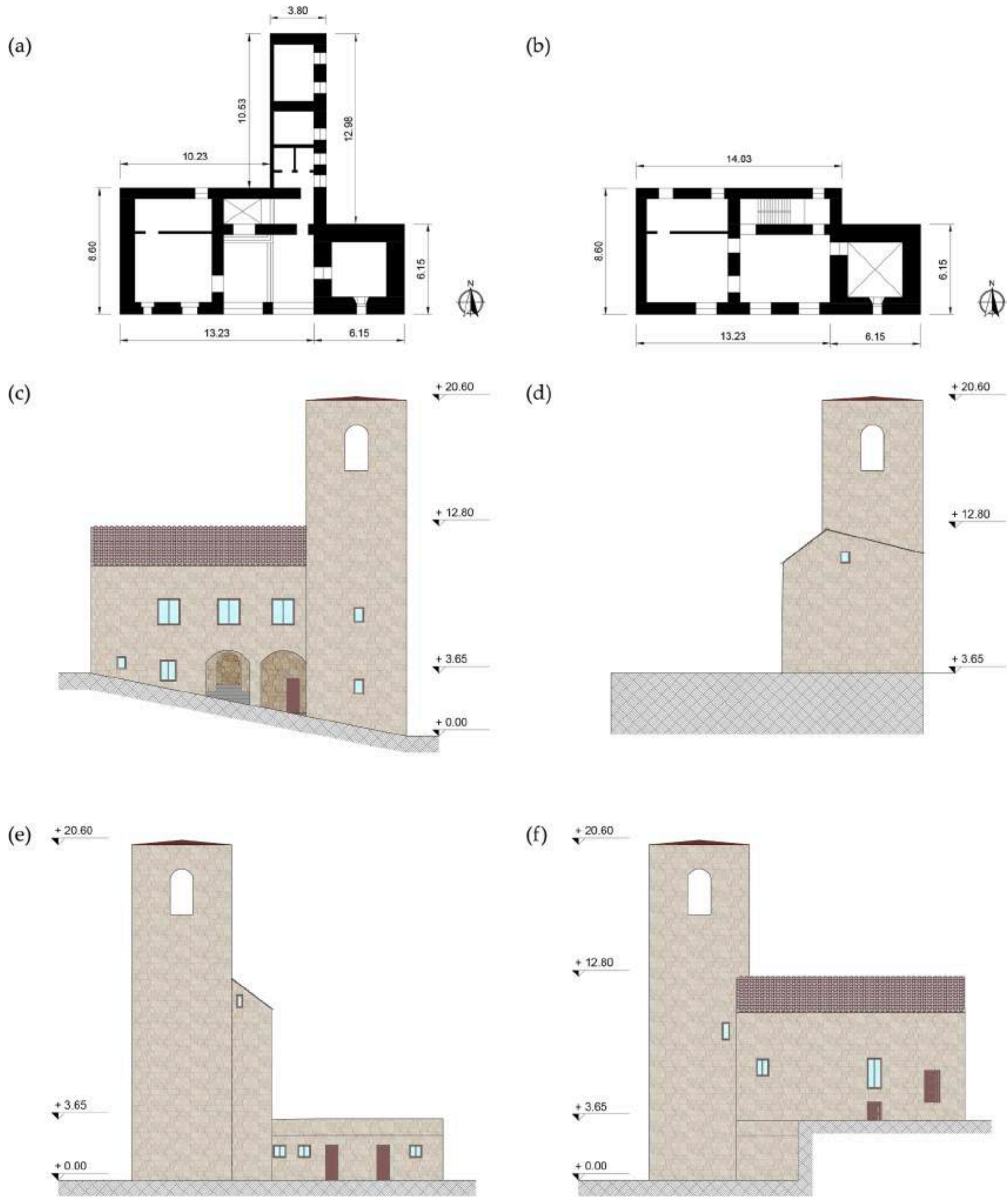

Fig. 2. The case study's ground and first floor layouts, as well as, the South, West, East, and North façades, are shown in (a), (b), (c), (d), (e), and (f) respectively. (All the dimensions are in meters).

corresponding to the bell-cell, and three embrasures along the height. Inside, there is one cross vault in masonry, whereas the pitched roof is made of reinforced concrete. The external masonry is characterized by regular stones. However, the walls' thickness suggests that inside there is an inner core of rubble stone.

The two floors of the Podestà Palace have a rectangular cross-section that measures 8.60 m × 14.00 m. The maximum building height is 12.80 m, which is evaluated at the ridge of the roof. The entrance, consisting of an arched portico is on the ground floor, while on the first floor there is the "Piano Nobile". The slabs are made of wood, except for a masonry cross-vault on the stairwell. The palace-bearing structure consists of regular stones.

On the south side, there is a one-floor annex with dimensions of 10.50 m × 3.80 m.

3. Damage suffered following the 2016–2017 Central Italy earthquake

After the seismic sequence recorded in Central Italy in the 2016–2017 period, the structure has presented deep cracks pattern. As reported in Fig. 3, the tower was the portion most involved in the damage: a torsion-flexural deformation on its upper part, sub-horizontal cracks, masonry disaggregation on the roof's support surface, and spread diagonal cracks in each bell-cell corner. These latter cracks represent rather clear evidence of the activation of out-of-plane processes. Small cracks also emerged through the Podestà Palace to the

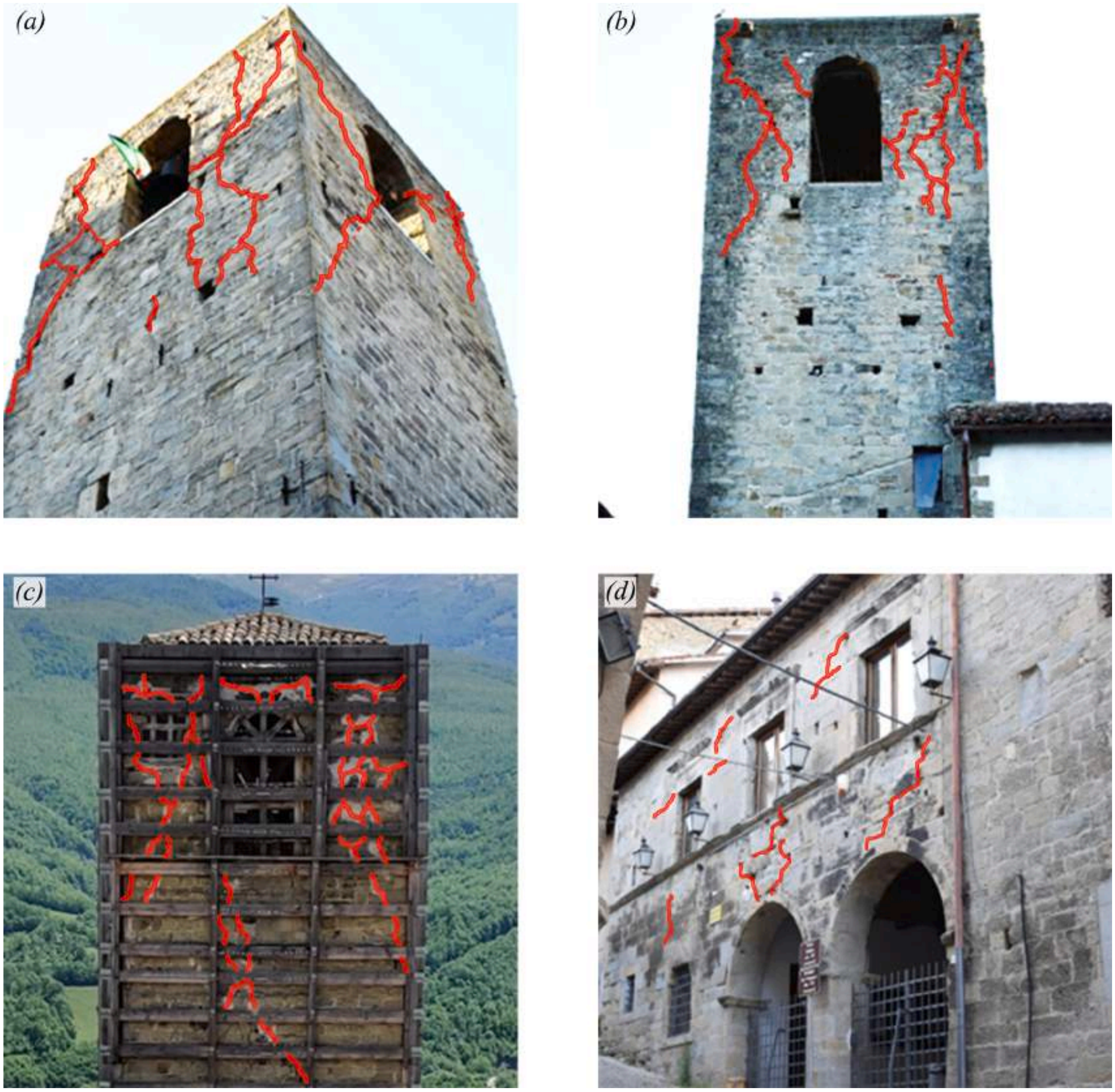

Fig. 3. Damage suffered by the structure following the Central Italy Earthquakes. Bell-cell (a) South-East, (b) North and (c) West façade; (d) Podestà Palace South façade.

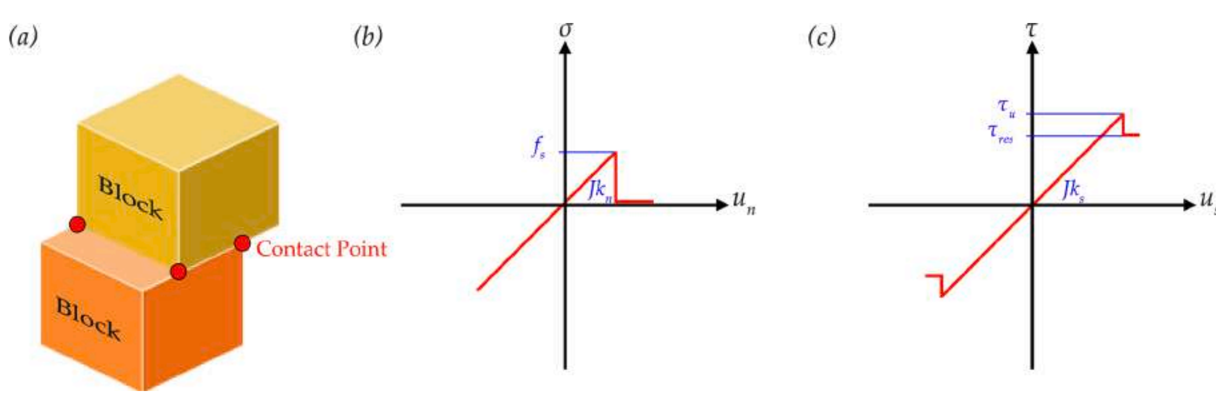

Fig. 4. Mechanical representation of contact point between blocks (a), laws in the normal (b) and the shear (c) directions.

tower connection, and between the portico's openings.

Before the last strong quake occurred on the 30th of October, this tower had been secured thanks to the firefighters by enclosing it with a system of ties and wood elements to avoid its collapse, as possible seismic sequences would have happened afterward.

4. Numerical models

The structure under investigation was analyzed with discontinuous and continuous models, respectively reported in the text with the acronyms DM and CM.

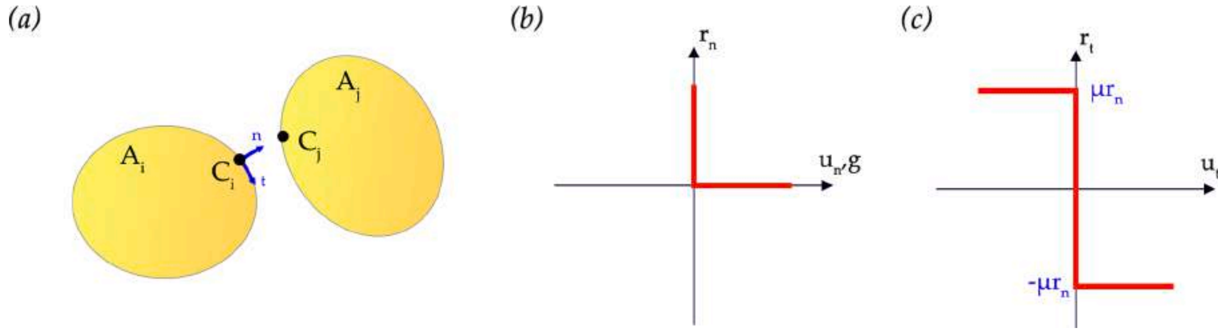

Fig. 5. Contact between bodies (a), Signorini's law (b) Eq. (6), and dry-friction Coulomb's law (c) Eq. (7).

The discontinuous models were simulated with both the 3DEC© [36] and the LMGC90© [37,38] software. The structural geometry was developed as a discrete block assembly. Since this model represents a simplified micro modelling approach, the blocks' dimensions included the mortar thickness. The existing pattern was replicated through the blocks, with sufficient accuracy. The non-linearity of masonry, concentrated in the interaction between blocks, was considered by the Discrete Element Methods (DEM) and the Non-Smooth Contact Dynamic (NSCD) method on the 3DEC© and LMGC90©, respectively.

On the other hand, a continuous FEM model was implemented with the commercial software Midas FEA NX© [39]. The masonry was simplified with a homogeneous isotropic material. Its non-linearity was considered with the Concrete Damage Plasticity Method (CDP) [40], as a setting option within the FEM. The CDP allows catching the cracking and the crashing simultaneously through the definition of distinct stress–strain and the damage-strain laws in tension and compression [41–44].

In the following paragraphs, the theories of the DEM, NSCD, and CDP are summarized.

4.1. The discrete Element Methods (DEM)

The DEM is implemented in the 3DEC© code [36] and represents the structure as a set of rigid or deformable blocks that interact one another through contact points. Conversely to the NSCD method, the DEM uses an explicit integration scheme using damping for its numerical stability. In this work, to compare the two discontinuous approaches, it was decided to use also rigid blocks for DEM.

The sliding between blocks is governed by linear and non-linear laws in the normal and shear directions. The blocks and the joints are constituted of internal particles (Fig. 4.a) connected through contact points. At these points, the movements are governed by contact laws (Fig. 4.b-c) thanks to a pair of springs that allow the normal and the shear forces transfer:

$$\Delta\sigma_n = Jk_n\Delta u_n \tag{1}$$

$$\Delta\tau_s = Jk_s\Delta u_s \tag{2}$$

In the breakage or in the traction occurrences, the cohesion and tensile strength are zero, and in parallel the friction angle remains unchanged.

When the shear force exceeds the value τ_{max}, the sliding takes place:

$$|\tau_s| \leq c+\sigma_n tan\phi = \tau_{max} \tag{3}$$

If the normal tension exceeds the shear strength:

$$if\ \ \sigma_n < -\tau, \sigma_n = 0 \tag{4}$$

4.2. Non-Smooth contact dynamics model (NSCD)

The NSCD method implemented in the LMGC90© [37,38] integrates non-smooth contact laws by means of an implicit scheme. Two bodies, the A_i candidate and the A_j antagonist, and then their possible points of contact C_i and C_j are considered, with n the vector orthogonal to the point of contact C_i (Fig. 5.a). The distance between the two points of contact will be defined as:

$$g = (C_j - C_i)n \tag{5}$$

Likewise, two contact laws were used wherein the normal ($\dot{u}_n$) and the tangential ($\dot{u}_t$) velocity of C_j with respect to C_i, and the normal (r_n) and the tangential (r_t), in that order the reaction forces of A_i on A_j, were determined.

Signorini's law of impenetrability (Fig. 5.b), Eqs. (6) and (7), specify a perfect plastic impact, i.e. Newton's law returns a coefficient equal to zero. As a result of the impact, there are no bounces, in the case of stones and bricks there is a low coefficient of return, and for this reason, it can be neglected:

$$g \geq 0,\ r_n \geq 0,\ gr_n = 0 \tag{6}$$

$$\text{if } g = 0 \rightarrow \dot{u}_n \geq 0 \rightarrow r_n \geq 0 \rightarrow \dot{u}_n r_n = 0. \tag{7}$$

The dry-friction Coulomb's law (Fig. 5.c) is considered as follows:

$$|r_t| \leq \mu r_n : \begin{cases} |r_t|\langle\mu r_n \rightarrow \dot{u}_t = 0, \\ |r_t| = \mu r_n \rightarrow \dot{u}_t = -\lambda\dfrac{r_t}{|r_t|}. \end{cases} \tag{8}$$

where μ is the friction coefficient and λ is a positive real arbitrary number.

The equation of motion can be written in this way:

$$M\ddot{q} = f(q,\dot{q},t) + l \tag{9}$$

M is the masses matrix, $\ddot{q}$ is the acceleration, $f(q,\dot{q},t)$ is the vector of the internal and external discretized forces acting on the system, meanwhile l is the resultant of contact.

The couples that characterize each contact, ($\dot{u}_n$, $\dot{u}_t$) and (r_n, r_t), are governed by linear maps that depend on q respectively to the global vectors $\dot{q}$ and l.

The reactions l and the velocity $\dot{q}$ are discontinuous functions of the time given that (6) - (7) are non-smooth. The velocities are discontinuous and the equation (8) can be integrated into the time t. The equation of motion is integrated into time intervals $[t_i,\ t_{i+1}]$ in this way:

$$M\left(\dot{q}_{i+1} - \dot{q}_i\right) = \int_{t_i}^{t_{i+1}} f(q,\dot{q},t)dt + \bar{l}_{i+1} \tag{10}$$

Where $\bar{l}_{i+1}$ is the pulse in the interval time and $\dot{q}_{i+1}$ is the variable that approximates the right limit of the speed in the time $[t_{i+1}]$.

The reactions are approximated in the average of the pulse in $[t_i,\ t_{i+1}]$ in the global (10) and the local contact (6) - (7). The deformability of the blocks is neglected, obtaining the dynamic interaction between the elements by sliding and oscillating of the blocks.

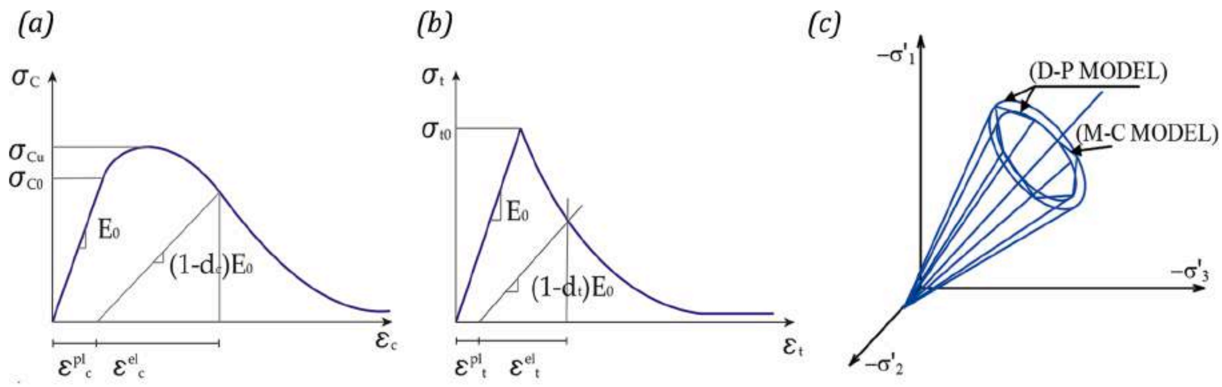

Fig. 6. Compression inelastic mono axial curve (a), Tensile inelastic mono axial-curve (b), Yield surface in the Westergaard space (c).

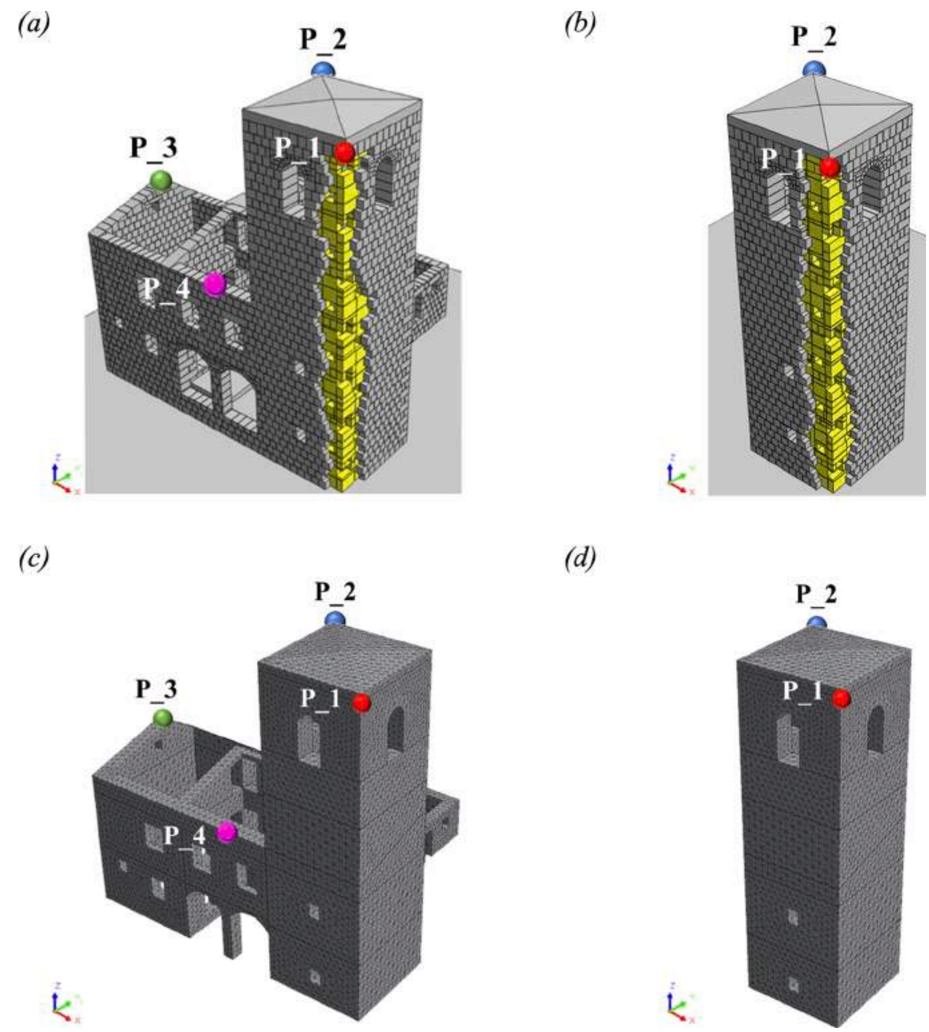

Fig. 7. Discontinuous (a)-(b) and Continuous (c)-(d) models of the entire building and of the tower alone. On them, the control points employed to plot the results are shown.

4.3. Concrete damage Plasticity model (CDP)

The masonry non-linearity in the continuous model was governed by the Concrete Damage Plasticity model (CDP) implemented in Midas FEA NX© [39]. Firstly, the CDP model was formulated to model the brittle behavior of concrete, then, over the years, it has been able at catching all brittle materials responses, such as masonry. CDP is an isotropic plasticity model presented for the first time by Lubliner [45] and improved by Lee & Fenves [40], subsequently. The first formulation introduced the concept of distinct responses in tension and compression. Whereas the improvement was accomplished considering the stiffness recovery following the cracks' closing under cycle loads.

The damage is defined by the effective configuration. To determine this, the equivalence between tension stress in the undamaged (σ_0) and the damaged (σ) configurations must be imposed while taking the damage parameter into account (d), Eq.(11). It is written under the

Table 1
Joints' parameters used in 3DEC© and LMGC90©.

Software	Parameters	Majority of contacts	Inner rubble masonry contacts
3DEC© LMGC90©	Friction [-]	0.50	0.30
3DEC©	Normal stiffness [N/mm^3]	7.67 E^9	2.67 E^{10}
	Tangential stiffness [N/mm^3]	3.07 E^9	1.07 E^{10}
	Cohesion [-]	0.10 E^6	
	Tensile strength [N/mm^2]	0.10 E^6	

hypothesis of strain equivalence, Eq.(12):

$$\boldsymbol{\sigma} = d \cdot \boldsymbol{\sigma_0} \tag{11}$$

$$\boldsymbol{\varepsilon} = \boldsymbol{\varepsilon}_0 \tag{12}$$

The strain tensor can be expressed as the sum of its elastic and plastic components, being the CDP a classical plasticity model:

$$\boldsymbol{\varepsilon} = \boldsymbol{\varepsilon}^e + \boldsymbol{\varepsilon}^p \tag{13}$$

where the elastic stress can be written as a function of the elastic damage stiffness matrix $\boldsymbol{E}$ using Hook's law:

$$\boldsymbol{\sigma} = \boldsymbol{E}\,(\boldsymbol{\varepsilon} - \boldsymbol{\varepsilon}^p) \tag{14}$$

To consider the damage irreversibility, the degraded stiffness matrix is expressed as:

$$\boldsymbol{E} \; = (1-d)\,\boldsymbol{E_0} \tag{15}$$

where $\boldsymbol{E}_0$ identifies the undamaged elastic stiffness matrix. During the elastic phase, d is equal to zero, then achieving to the value of one at the complete rupture of that material. Due to this consideration, the relationship between stress and strain becomes as follows:

$$\boldsymbol{\sigma} = (1-d)\boldsymbol{E}_0(\boldsymbol{\varepsilon} - \boldsymbol{\varepsilon}^p) \tag{16}$$

Two different damaged variable laws must be defined in tension and compression, as reported in Eqs. (17) and (18), for considering the higher stiffness degradation in tension (d_t) compared to that in compression (d_c), under mono axial stress (Fig. 6.a-b). They assume increasing values as the elastic strain increases:

$$\sigma_t = (1-d_t)\,E_0\left(\varepsilon_t - \varepsilon_t^p\right) \tag{17}$$

$$\sigma_c = (1-d_c)\,E_0\,\left(\varepsilon_c - \varepsilon_c^p\right) \tag{18}$$

Conversely, the crack closure observed under the cyclic loading phase is considered as a contribution to a partial elastic stiffness recovery, especially passing from tension to compression status. In this case, it is assumed that:

$$(1-d) = (1-s_t d_c)(1-s_c d_t) \tag{19}$$

The s_t and s_c are used to consider the stiffness recovery during the load inversion stage, dependent on weight factors:

$$s_t \; = 1 - w_t r^*(\widehat{\overline{\sigma}}), \tag{20}$$

Table 2
Materials parameters used in the continuous model.

	Medium-quality masonry properties	Low-quality masonry properties	Concrete
Young's modulus [N/mm^2]	2800		31500
Poisson's modulus, ν	0.25		0.30
Mass [kN/m^3]	22		25
Strength in compression [N/mm^2]	8.0	5.6	–
Strength in tension [N/mm^2]	1.6	0.46	–
Parameters to define the CDP Yield surface			
Dilatation angle, ψ	10°		–
Correction parameter, k_c	0.666		–
Eccentricity, ε_{eccen}	0.1		–
Biaxial strength ratio, f_{b0}/f_{c0}	1.16		–
Viscosity, μ	0.01		–

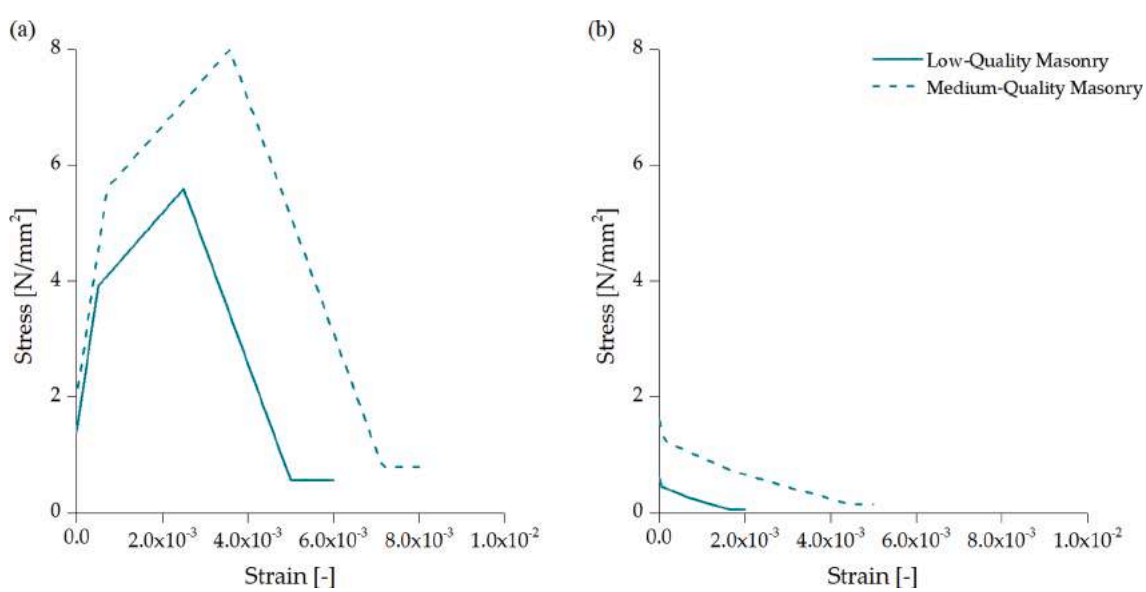

Fig. 8. CDP constitutive laws defined in compression (a) and tension (b).

Table 3
The main parameters of the three quakes considered.

Seismic Event	ML	Depth (km)	Station	Class EC8	Rjb (km)	Rrup (km)	Repi (km)	N-SPGA (m/s2)	E-WPGA (m/s^2)	ZPGA (m/s^2)
24/08/2016	6.0	8.1	AMT	B*	1.38	4.62	8.50	3.68	−8.51	3.91
26/10/2016	5.9	7.5	AMT	B*	25.9	26.1	33.30	−0.59	0.91	0.49
30/10/2016	6.1	9.2	ACC	A*	2.2	5.7	18.60	−3.95	4.34	−5.47

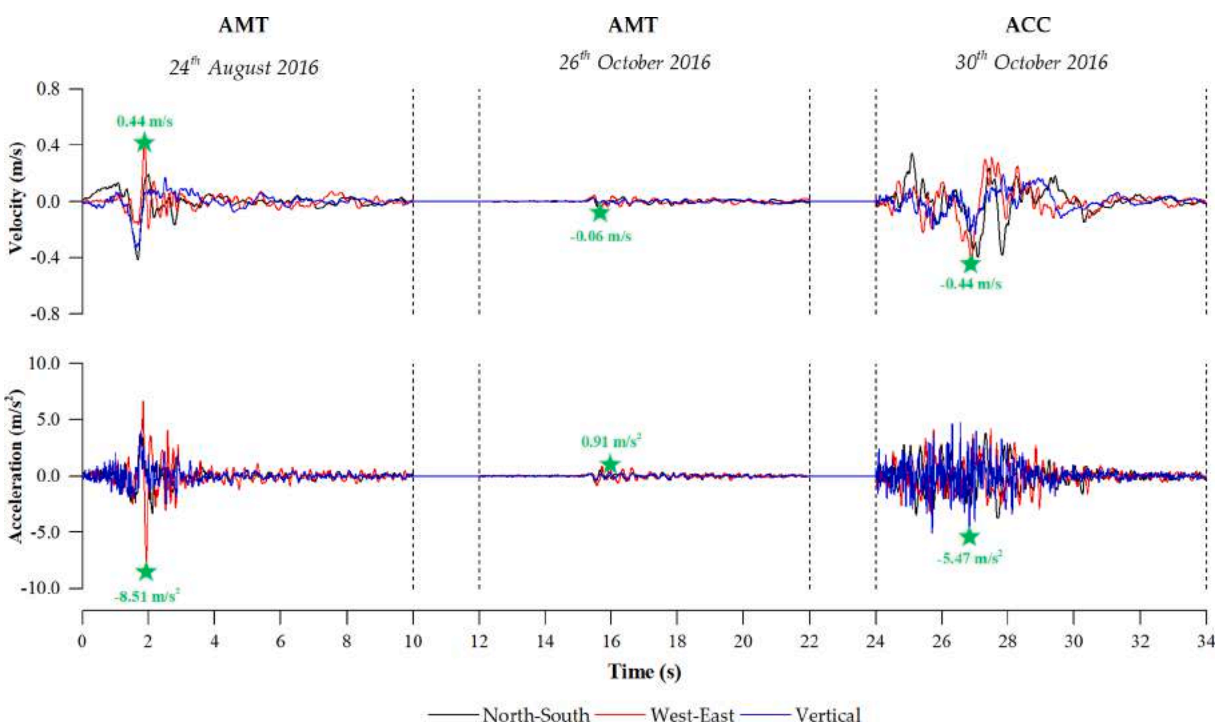

Fig. 9. Velocities and acceleration time histories applied to DM and CM, respectively.

$$s_c = 1 - w_c(1 - r^*(\hat{\overline{\sigma}})), \quad (21)$$

where $r^*(\hat{\overline{\sigma}})$ accounts for the values from zero to one range. This is equal to zero if the principal stresses are all positive. When the primary stresses are all negative, it takes on value.

The w_t and w_c values are defined to consider the stiffness recovery. If they are zero, stiffness recovery is not considered. On the other hand, if they are equal to one, it means that complete recovery is achieved.

To define the boundary of the elastic domain, a yield strength function based on the Drucker-Prager function is employed, (Fig. 6.c):

$$F(\overline{\sigma},\kappa) = \frac{1}{1-\alpha}\left[\alpha I_1 + \sqrt{3I_2} + \beta(\kappa)\langle\hat{\overline{\sigma}}_{max}\rangle - \gamma\langle -\hat{\overline{\sigma}}_{max}\rangle\right] - c_c(\kappa) \quad (22)$$

with:

I_1 the first invariant of effective stress;

I_2 the second invariant of effective stress;

$\hat{\overline{\sigma}}$ Maximum principal effective stress.

Whereas α and β are two constants determined using the initial uniaxial compressive yield stress f_{b0} and the initial equiaxial compressive yield stress f_{c0} as:

$$\alpha = \frac{f_{b0} - f_{c0}}{2f_{b0} - f_{c0}} \quad (23)$$

$$\beta = \frac{c_c(\kappa)}{c_t(\kappa)}(\alpha - 1) - (1 + \alpha) \quad (24)$$

and $c_c(\kappa)$ and $c_t(\kappa)$ are the effective cohesion in compression and in tension, respectively.

Finally, the constant γ is calculated as:

$$\gamma = 3\frac{1 - k_c}{2k_c - 1} \quad (25)$$

In detail, $k_c = I_{2,TM}/I_{2,CM}$ is the ratio of the second stress invariant on the tensile median ($I_{2,TM}$) to that on the compressive meridian ($I_{2,CM}$) at the initial yield. The CDP modeled the non-associated potential flow employing the Drucker-Prager hyperbolic function. It is defined by the dilatation angle (ψ), the eccentricity ε_{eccen}, and the tensile strength f_{t0}:

$$G = \sqrt{(\varepsilon_{eccen} f_{t0}\tan\psi)^2 + 3I_2} + \frac{1}{3}I_1\tan\psi\,. \quad (26)$$

4.4. Numerical models characteristics

The structural geometry was precisely reproduced in both approaches (Fig. 7) paying attention to each element and opening. The boundary conditions at the ground floor were defined to take into account the ground presence on the walls by adding big blocks and vertical rollers adjacent to them in the DMs and the CM, respectively.

In order to investigate the influence of the Podestà Palace presence on the tower damage, two models were built for each approach: the first one for the entire complex and the second only for the tower.

The DMs' geometries counted 6790 blocks for the entire construction and 4021 blocks (Fig. 7**.a)** for the isolated tower (Fig. 7**.b)**. The tower walls' thicknesses were split into three parts to distinguish the external layers, of 0.40 m each, from the inner core, of 0.40 m, as highlighted in yellow in Fig. 7**.a**. The inner core was modeled by pulling its blocks close to those comprised in the external perimeter. A cross-sectional diatone

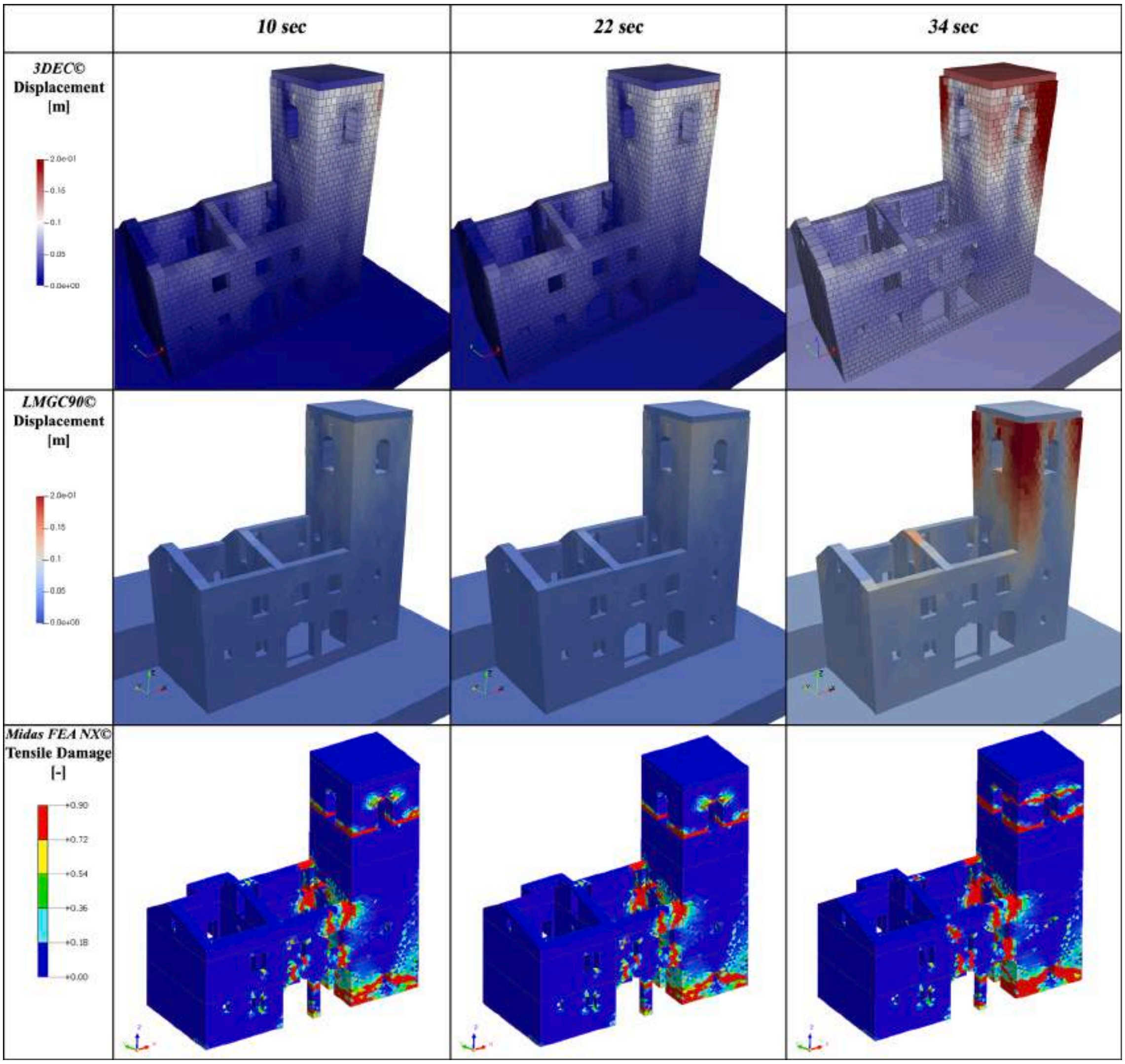

Fig. 10. Damage at the end of each event obtained with 3DEC©, LMGC90©, and Midas FEA NX© analyzing the whole structure.

was inserted every square meter, ensuring a limited connection between the wall's layers.

The CM's geometries were discretized with 3D 4-node tetrahedral elements with an average dimension of 0.40 m. The whole structure model (Fig. 7**.c)** contained 29,986 elements, 23,091 nodes, and 69,276 degrees of freedom, whereas the tower alone (Fig. 7**.d)** had 57,780 elements, 13,123 nodes, and 39,372 degrees of freedom.

Distinct parameters are required to simulate the masonry behavior. In the DMs, if the density was the only parameter assigned to the blocks, the parameters defined for their interactions were different based on the related laws implemented in the approaches. Moreover, only joints' friction values were required for the NSCD developed within the LMGC90©. Whereas the DEM employed in the 3DEC© needed the additional definition of the normal and shear stiffness, cohesion, and tensile strength of joints.

The models implemented with the Midas FEA NX© need the definition of the Young's moduli, the Poisson's moduli, and the masses for the linear response. On the other hand, regarding the mechanical non-linearity of masonry, the parameters of the yield surface and the two mono-axial laws in tension and compression with their respective damage evolutions should be determined.

The materials' parameters were reported as those referenced in the Italian Code [46,47].

In the DMs, the density of the cut stone, 2200 kg/m^3, was assigned to the structure, except for the inner rubble masonry and the roof, assuming densities of 1900 kg/m^3 and 2500 kg/m^3, respectively. As reported in previous studies [48–50], the joints' friction was specified as follows: 0.9 is the value imposed between the blocks and the ground; 0.3 is applied both between the inner rubble masonry of the tower, and at the contact surface of the inner rubble masonry and the external layers of the tower (including the blocks crossing the entire wall's thickness). Then, the friction accounts for a value of 0.5 between the remaining blocks. Finally, the additional parameters specified in 3DEC© are collected in Table 1.

On the other hand, in the CM, three materials were considered: one for the complex and tower body, another one for the bell cell, and the last one for the roof. Observing the structures and the cracks that occurred, there has been evidence in the good quality of the masonry not only in the Podestà Palace and annex but also in the tower body even if with a multi leaf masonry. This is the reason why 'Medium-quality masonry properties' (see Table 2) was assigned to the material. Conversely, due to its exposition to the atmospheric agents, the bell cell showed a reduction of the mortar in the joints, which was simulated by lowering its non-linear parameters ('Low-quality masonry properties' in Table 2**)**. Finally, the elastic parameters of the concrete were assigned for the roof modelling. The non-linear parameters of the concrete were not defined as no damage was observed on the roof during the earthquakes. The mono-axial tensile and compressive laws, wherein the

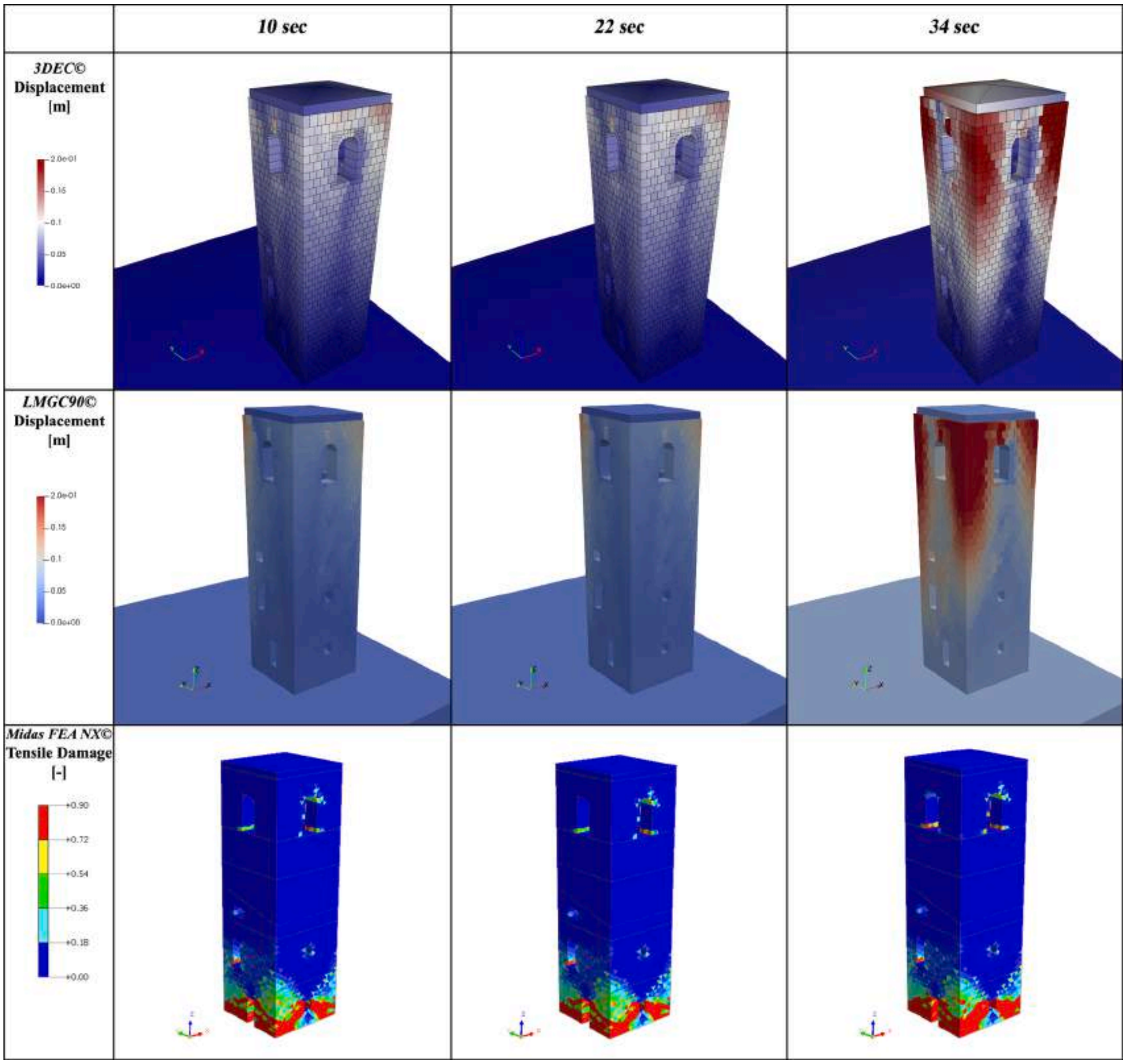

Fig. 11. Damage at the end of each event obtained with 3DEC©, LMGC90©, and Midas FEA NX© analyzing the tower alone.

damage variables were considered in a range from 0 to 0.9 to avoid computational instability, are shown in Fig. 8. The yield surface parameters employed are collected in Table 2**.**

The models underwent non-linear dynamic analyses. The three main shocks that occurred in 2016 on August 24^{th}, October $26^{th,}$ and 30^{th} were analyzed. The accelerations and the velocities recorded, the first two in Amatrice and the last one in Accumoli, were applied at the discontinuous and the continuous models' base, respectively. In particular, the data were given from the station in Amatrice for the first two sequences, due to its better quality in signal recording than the ones registered in Accumoli, and for its proximity to this case study's site.

The main parameters of the aforementioned earthquakes [51] are collected in Table 3. Class EC8 indicates the type of ground on which the earthquake was recorded; R_{jb} is the Joyner-Boore distance, or rather the smallest spacing between the rupture site and the rupture surface projection; R_{rup} is the shortest distance between the rupture site and the rupture surface; R_{epi} is the distance calculated by the geometric swap.

To expedite the computational procedure, only 10 seconds of each earthquake's strong motion were taken into account. Then, they were attached in a series, spaced out by a two-second rest, for a total time of 34 seconds (Fig. 9). All the spatial three directions were considered. The analysis is performed with a 0.005-second load step setting. Morever, the damping was used in the 3DEC© code to decrease false oscillations originating from the explicit nature of the time integration technique and to reach the state of equilibrium of forces as quickly as possible. Thus, a local damping was used for the Palace and Tower analyses using a value of 5%. Conversely, the LMGC90© code neglected the damping effects and the dissipated energy was related to the contribution of the friction. Finally, in the MIDAS FEA NX©, the damping was determined using the Rayleigh method considering the 1^{st} and 77^{th} modes and a damping of 3% [26]. The 77^{th} mode was selected so as to reach a value of 85% for the participation mass, along both the X and Y directions.

5. Results

The numerical models' results are compared in Fig. 10 and Fig. 11 in terms of blocks' sliding and masonry's tensile damage, for the DM and CM respectively, and in terms of displacements time histories in Fig. 12, Fig. 13, Fig. 14 and Table 4, Table 5. In the CDP the compressive damage was unplotted being irrelevant in the masonry structures response. Four control points along the external roof's perimeter were considered: two on the tower (P_1 and P_2), and two on the palace (P_3 and P_4), as shown in Fig. 7.

The time histories of the whole system (actual configuration) have similar trends for each approach utilized (Fig. 12, Fig. 13, and Fig. 14 and Table 4). The major displacements are recorded on the tower, corresponding to the P_1 and P_2 points, in both the X and Y directions. Their largest residual displacements were measured at the end of August

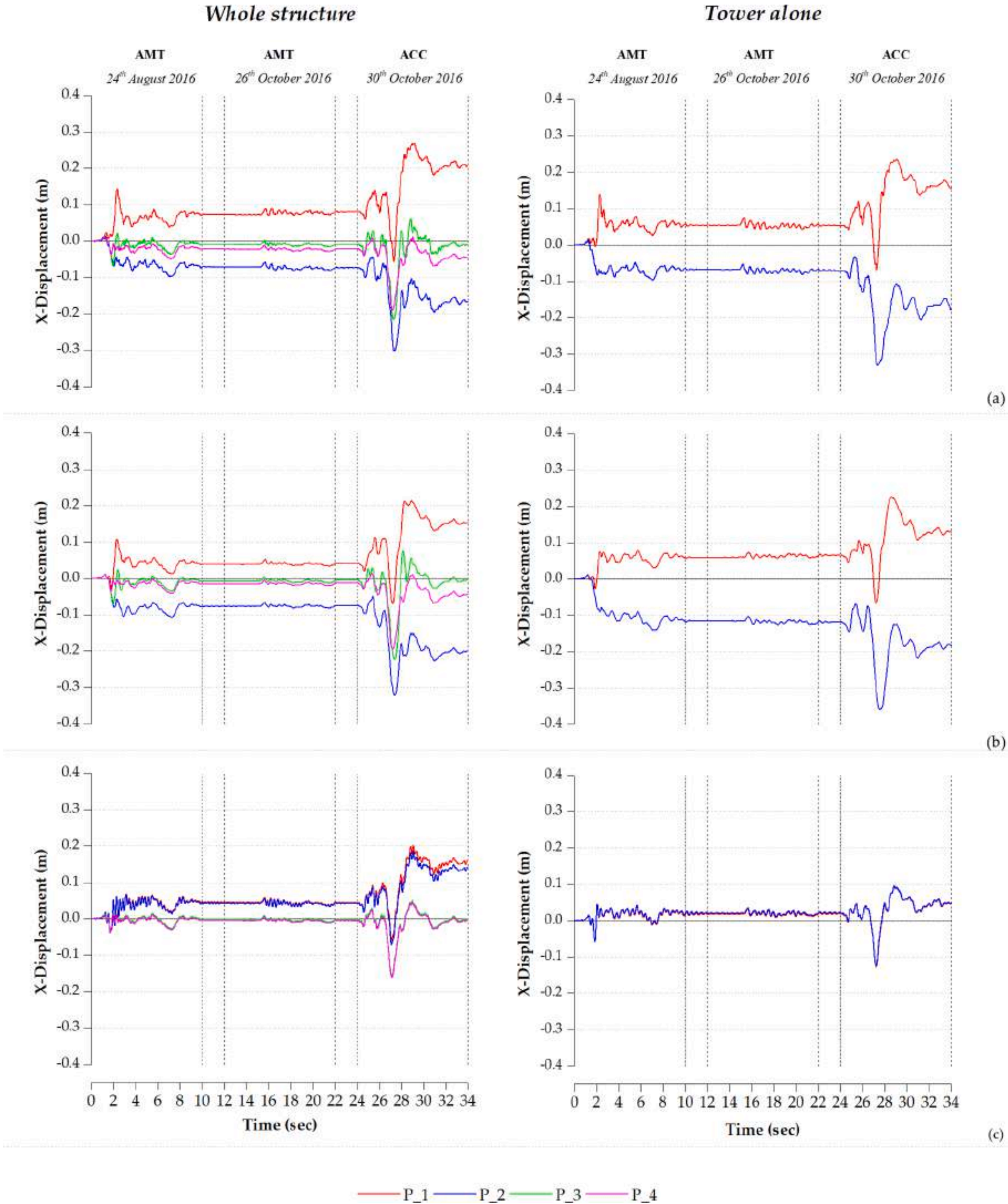

Fig. 12. Comparison between the whole complex and the tower alone X-displacement's time histories, obtained with 3DEC© (a), LMGC90© (b), and Midas FEA NX© (c).

24th and October 30th, contrary to the second event, during which the construction scenario had not modified (Fig. 12, Fig. 13 and Table 4). At the end of the August 24th sequence, the X/Y residual displacements of P_1 are equal to 0.07 m/-0.1 m in 3DEC© (Fig. 12**a**, Fig. 13**a** and Table 4), 0.04 m/-0.07 m in LMGC90© (Fig. 12**b**, Fig. 13**b** and Table 4), and 0.05 m/0.02 m in Midas FEA NX© (Fig. 12**c**, Fig. 13**c** and Table 4). Moreover, P_2 values are −0.07 m/0.02 m 3DEC© (Fig. 12**a**, Fig. 13**a** and Table 4), −0.08 m/0.01 m LMGC90© (Fig. 12**b**, Fig. 13**b** and Table 4), and 0.05 m/0.01 m in Midas FEA NX© (Fig. 12**c**, Fig. 13**c** and Table 4). Contrary to the second event, during which the construction scenario had not modified, after the October 30th earthquake the structural damage had increased. At the end of the sequence, the residual displacements (X/Y) of the P_1 are 0.21 m/-0.20 m in 3DEC© (Fig. 12**a**, Fig. 13**a** and Table 4), 0.15 m/-0.13 m in LMGC90© (Fig. 12**b**, Fig. 13**b** and Table 4), and 0.05 m/0.08 m in Midas FEA NX© (Fig. 12**c**, Fig. 13**c** and Table 4). However, the ones (X/Y) measured in P_2 are −0.17 m/0.06 m in 3DEC© (Fig. 12**a**, Fig. 13**a** and Table 4), −0.20 m/0.10 m in LMGC90© (Fig. 12**b**, Fig. 13**b** and Table 4), and 0.05 m/0.06 m in Midas FEA NX© (Fig. 12**c**, Fig. 13**c** and Table 4). These results are also confirmed by the damage plots at the end of each event reported in

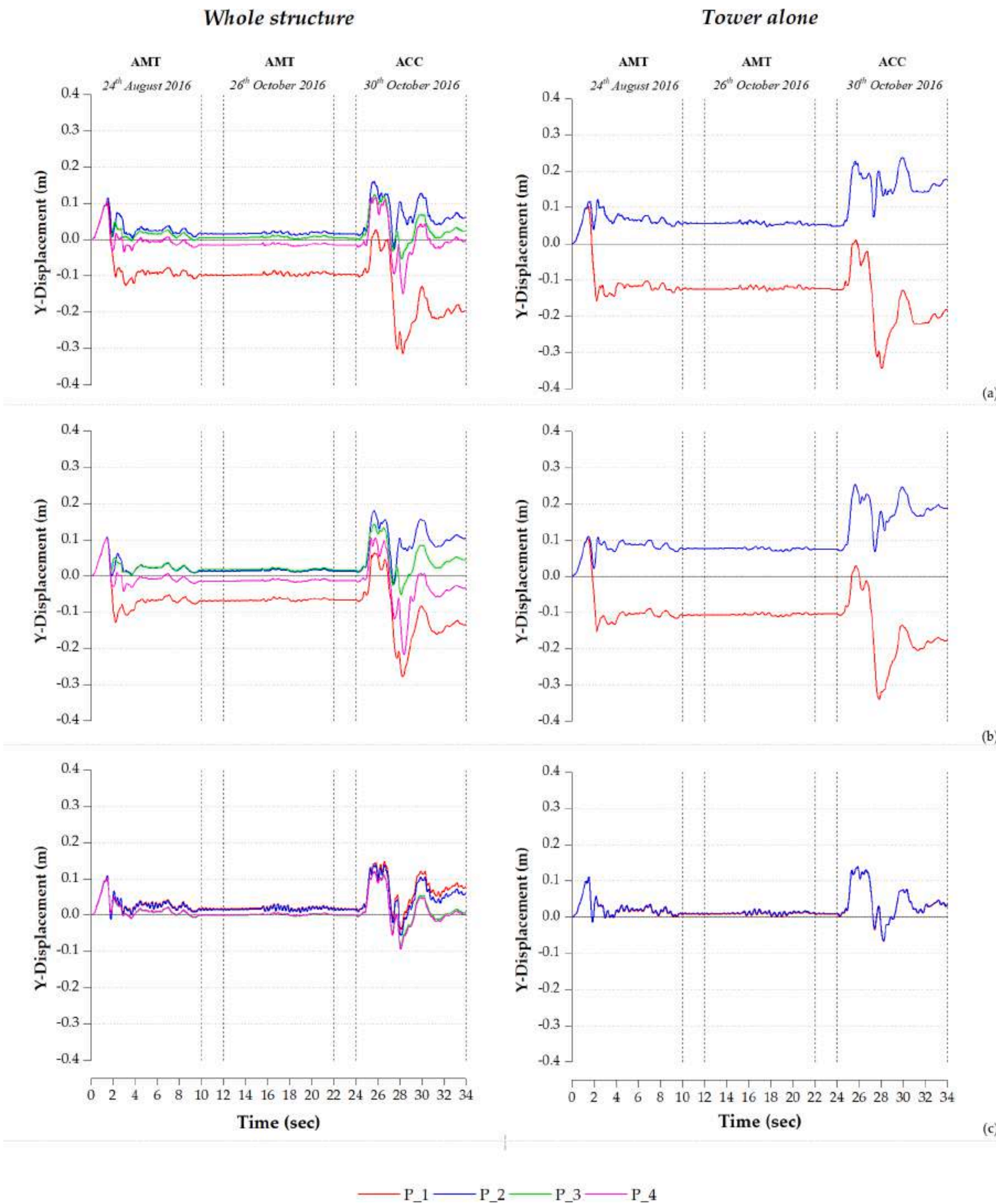

Fig. 13. Comparison between the whole complex and the tower alone Y-displacement's time histories, obtained with 3DEC© (a), LMGC90© (b), and Midas FEA NX© (c).

Fig. 10.

Whilst the DMs' results record very similar values, differences are detected than to the CM (Fig. 12, Fig. 13 and Table 4). Indeed, the discontinuous formulations allow the blocks to move in opposite directions, in contrast with the CM ones. As a result, numerical damage is affected by those conditions: if on one hand in the DMs the starting of the out-of-plane mechanisms of the tower's angles is observed, on the other hand, the cracked phase of the CM is characterized by the occurrence of the horizontal failure with a progressive development from the upper part of the arched windows to the corners.

Concerning the Podestà Palace, the displacements are smaller than the tower ones. For the DMs, the residual displacements stay in a range of 0.003 m and 0.01 m considering the values in modulus (Fig. 12**a-b**, Fig. 13**a-b** and Table 4), and close to zero in the CM after the process duration of 34 s (Fig. 12**c**, Fig. 13**c** and Table 4). On such structure's portion, the damages showed by DMs and CM are comparable. Cracks are collocated between the entrance openings and in the tower-to-palace connection like the actual ones (Fig. 15). On the other hand, the residual displacements of the only tower in the CM result lower than those of the entire structure. Indeed, the percentage of the completely damaged

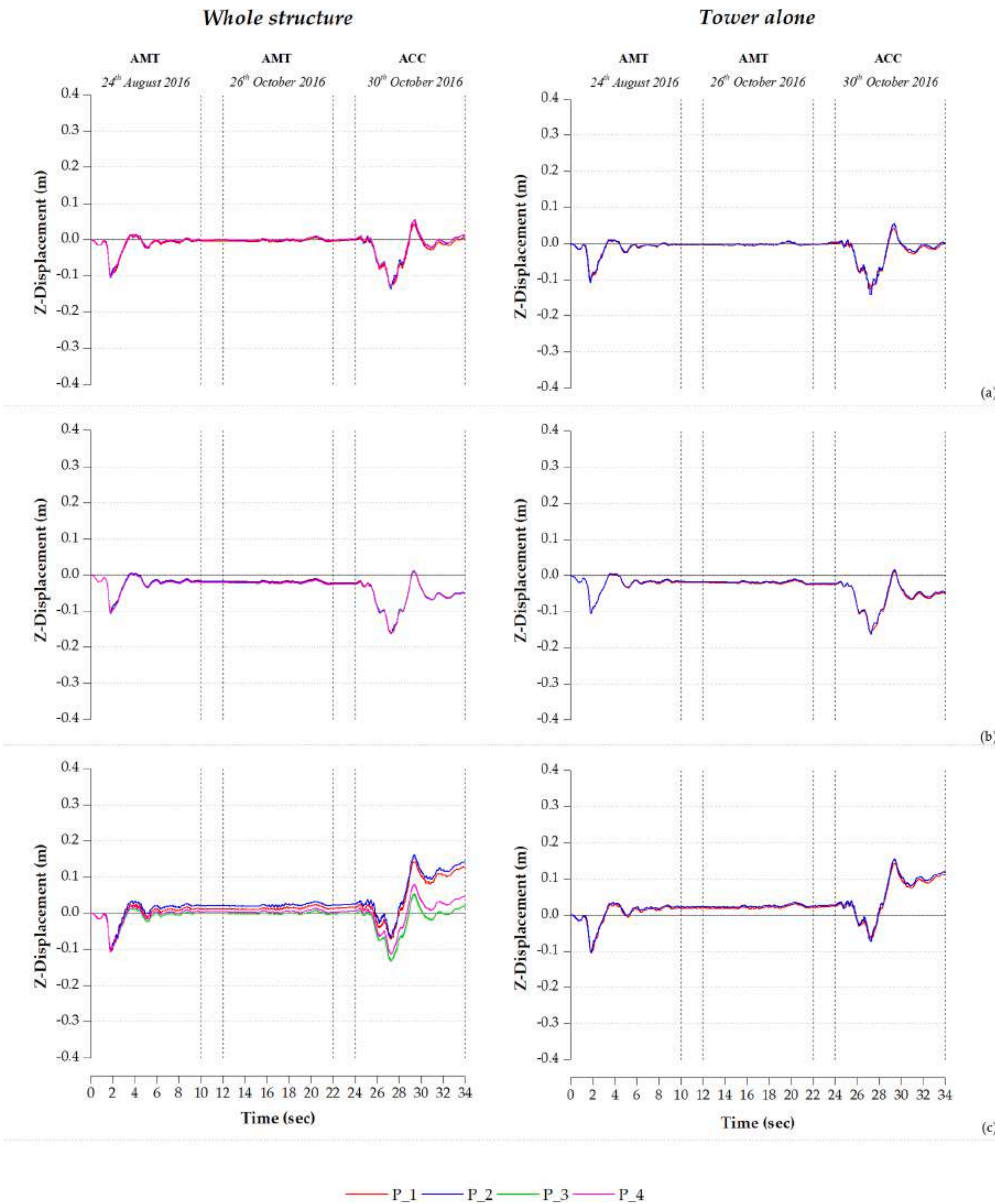

Fig. 14. Comparison between the whole complex and the tower alone Z-displacement's time histories, obtained with 3DEC© (a), LMGC90© (b), and Midas FEA NX© (c).

volume in the tower is 4.5% when it is isolated, and 10.4% when the palace is included. Observing the graphs in the DMs, a fast evaluation of that should not be taken. In the X-Direction, the residual deformations of P_1 are reduced (Fig. 12**a** and Table 5) while those of P_2 are similar to the whole structure ones (Fig. 12**a** and Table 5). Otherwise, along the Y direction (Fig. 13 and Table 5), larger displacements are measured for both points than in the previous analyses, except for that of P_1 obtained with the LMGC90©, which is slightly lower (Fig. 13**b** and Table 5). Comparison of the resultant displacements in the X-Y plane with those of the previous model reveals if the tower itself reported major or minor residual displacements at the sequence ending. In the whole model, these displacements register in P_1(P_2) the measurement of 0.29(0.18) m and 0.20(0.22) m respectively using 3DEC© and LMGC90©. In parallel, the tower modelling reports in P_1 the values of 0.24 m and 0.22 m, and in P_2 0.25 m and 0.26 m. According to these resultant displacements, on condition that the tower was isolated, the angles would have suffered from greater displacements, especially the P_2 reference point. Therefore, it should be clear the crucial role of the palace in the reduction of the walls' opening (Fig. 10): indeed, in this case, the hinges' formation occurs at the upper part of the attached tower, corresponding

Table 4
Whole structure: Summary displacement values at the end of each event (all values are expressed in meters).

		24/08/2016			26/10/2016			30/10/2016		
		X	Y	Z	X	Y	Z	X	Y	Z
3DEC©	P_1	0.07	−0.10	0.00	0.08	−0.10	0.00	0.21	−0.20	0.00
	P_2	−0.07	0.02	0.00	−0.07	0.01	0.00	−0.17	0.06	0.01
	P_3	−0.01	0.00	0.00	−0.01	0.00	0.00	0.00	0.02	0.01
	P_4	−0.01	−0.02	0.00	−0.01	−0.02	0.00	−0.05	0.00	0.01
LMGC90©	P_1	0.04	−0.07	−0.01	0.04	−0.07	−0.02	0.15	−0.13	−0.05
	P_2	−0.08	0.01	−0.01	−0.08	0.01	−0.02	−0.20	0.10	−0.05
	P_3	−0.01	0.01	−0.02	−0.01	0.01	−0.03	0.00	0.04	−0.05
	P_4	−0.01	−0.01	−0.02	−0.01	−0.01	−0.03	−0.04	−0.03	−0.05
MIDAS FEA NX©	P_1	0.05	0.02	0.01	0.04	0.02	0.02	0.05	0.08	0.13
	P_2	0.05	0.01	0.02	0.04	0.02	0.02	0.05	0.06	0.14
	P_3	0.00	0.00	0.00	0.00	0.00	0.00	0.00	0.01	0.02
	P_4	0.00	0.00	0.00	−0.01	0.00	0.01	0.00	0.00	0.04

Table 5
Tower alone: Summary displacement values at the end of each event (all values are expressed in meters).

		24/08/2016			26/10/2016			30/10/2016		
		X	Y	Z	X	Y	Z	X	Y	Z
3DEC©	P_1	0.05	−0.13	−0.01	0.05	−0.13	0.00	0.14	−0.18	0.00
	P_2	−0.07	0.05	−0.01	−0.07	0.05	0.00	−0.18	0.17	0.00
LMGC90©	P_1	0.06	−0.11	−0.02	0.06	−0.11	−0.03	0.13	−0.18	−0.05
	P_2	−0.11	0.08	−0.02	−0.12	0.07	−0.03	−0.18	0.19	−0.05
MIDAS FEA NX©	P_1	0.02	0.01	0.02	0.02	0.01	0.03	0.05	0.03	0.11
	P_2	0.02	0.01	0.02	0.02	0.01	0.03	0.05	0.03	0.12

to the corners where the out-of-plane mechanism is activated, and they are definitely higher than in the single tower, as shown in Fig. 11. Whereas the cracks on CM are localized at the base since it shows the classic cantilever beam behaviour where the shear stress is maximum at the interlocking, and progressively decreases moving far away from it, as visible in Fig. 11. As a result, the cracks on the bell cell are fewer than those identified with the whole complex and then they are incoherent with reality, as shown in Fig. 16.

6. Conclusions

In this paper, an important structure damaged by the central Italian seismic sequence that occurred between 2016 and 2017 was analyzed. The structural response during this event was simulated by considering the whole structure and the tower alone in order to understand what extent the palace's presence affected the tower's damage. To this aim, three different approaches were employed. Masonry was represented as a continuous medium in one of them, and the non-linearity was assigned with different constitutive laws in tension and compression. In the others, it was modeled as an assembly of discrete blocks, and the non-linearity was assigned to their interactions. The two approaches used to implement the discontinuous models employed different interaction laws, one smooth and one non-smooth. The earthquake was simulated in all the models with non-linear dynamic analyses applying the three main events recorded in the proximity of the case study. To reduce the computational time, only ten-second interval of strong motion was considered for each analysis (Table 6). The elaborations in 3DEC© and MIDAS FEA NX© were carried out on a 64–bit Windows 10 computer with 512 Gb RAM, an Intel Xeon Gold 6130 CPU running at 2.10 GHz and 64 threads. As regard the LMGC90©, they were carried out on Ubuntu 16.04.3 LTS 64 bits, on a server machine Intel Core Processor 2.40 GHz, with 20 threads, and 64 GB of RAM. The analyses were run with multiple independent simulations in parallel, except for 3DEC© for which this cannot be done.

The results showed that using the smooth and the non-smooth laws for the blocks' interactions, the results were comparable for all the analyses performed. Both the DMs and the CM showed that in the real structural configuration, the points that suffered more damage were those on the upper part of the tower, having measured the largest residual deformation. Another vulnerable point identified by both of them was the palace section close to the tower that showed vertical cracks between the openings and in the connection palace-tower.

The numerical models' damage displayed that the DMs were able to retrace the real cracks present in the tower compared to the CM. Indeed, the cracks that occurred highlighted the activation of the out-of-plane mechanism of the tower's corners that can be identified only with DMs. It must be underlined that this behavior is commonly observed on old towers excited by quakes. On the other hand, both DM and CM simulated accurately the cracks caused by in-plane mechanisms that were visible in the building between the entrance openings and at the tower connection.

The study of the isolated tower led to additional considerations. DMs and CM react differently. The tower in the CM exhibited the typical behaviour of a cantilever beam cracking only near the base. This meant that the top relative displacements were less than in the previous condition. Instead, both DMs, particularly the one made with the LMGC90©, displayed higher irreversible displacement whereas the type of damage remained constant. In other words, as in the whole model, the DMs of the isolated tower were characterized by the activation of the corners overturning, which began at a lower height in this case.

This study demonstrated the importance of using the correct masonry modelling technique when analysing old masonry towers, particularly isolated ones. Indeed, due to their constant exposure to atmospheric agents and poor state of conservation, they frequently exhibit out-of-plane mechanisms that are unrepeatable using continuous FEM.

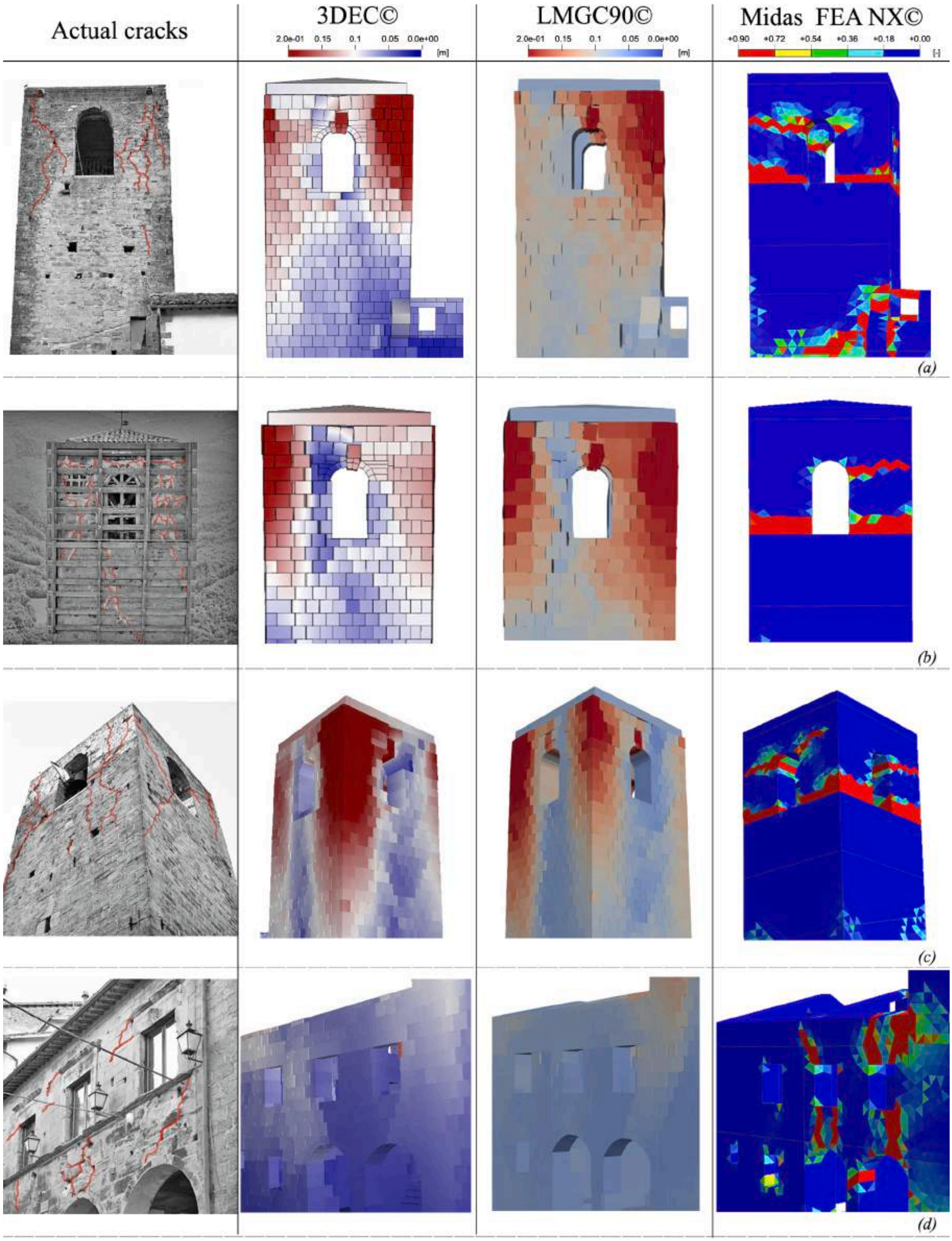

Fig. 15. Comparison of the actual cracks and the numerical damage, obtained with each software, for the whole structure. (a) Bell-tower North façade; (b) Bell-tower West façade; (c) Bell-tower South-East corner; (d) Podestà Palace south façade.

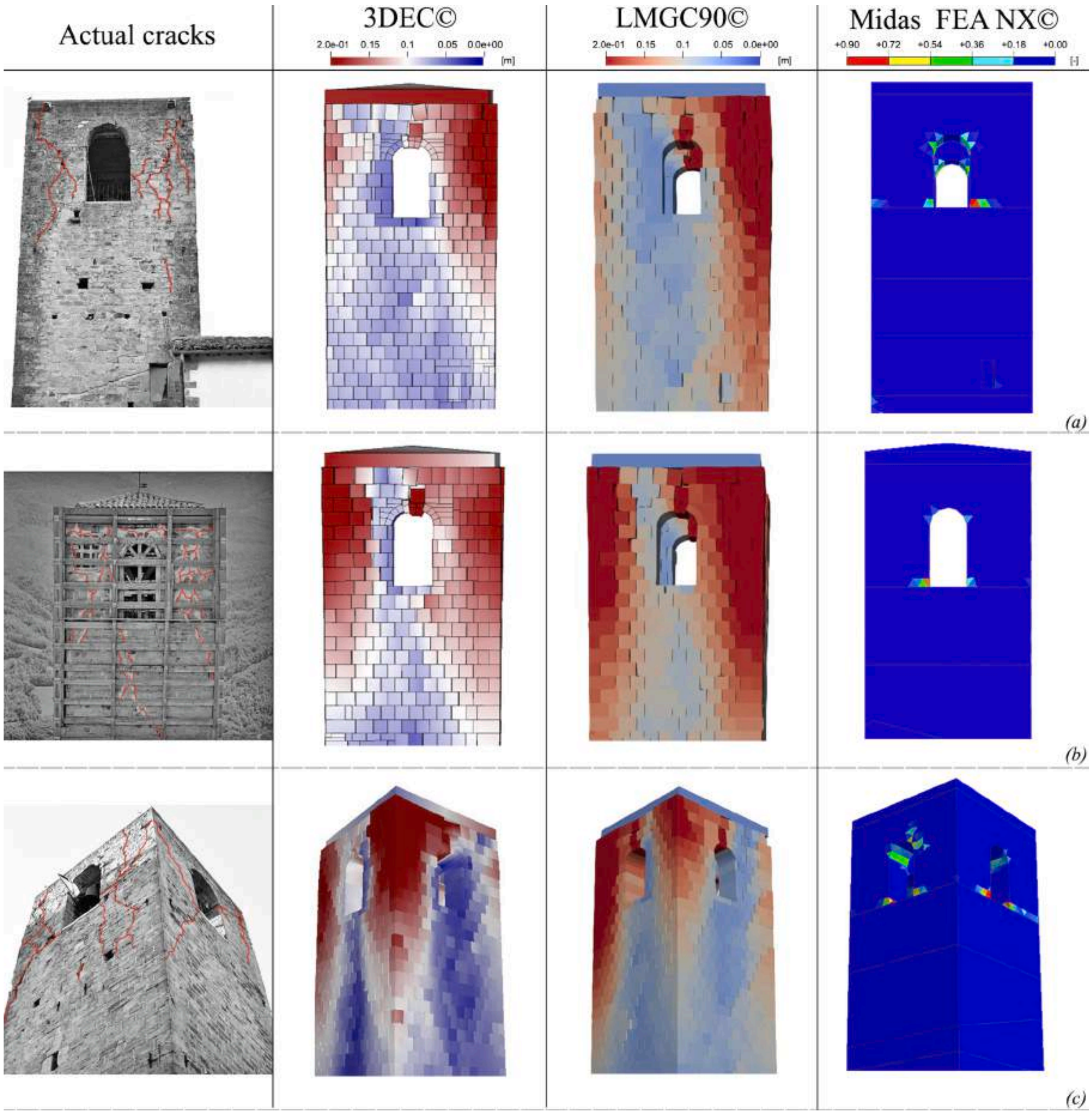

Fig. 16. Comparison of the actual cracks and the numerical damage, obtained with each software, for the tower alone. (a) Bell-tower North façade; (b) Bell-tower West façade; (c) Bell-tower South-East corner.

Table 6
Computational time for each analysis.

	Whole Structures	Tower Alone	n. of Threads
3DEC©	18 h 13 min	14 h 55 min	1
LMGC90©	286 h 00 min	67 h 25 min	20
MIDAS FEA NX©	18 h 13 min	14 h 55 min	50

CRediT authorship contribution statement

Mattia Schiavoni: Visualization, Writing – original draft, Data curation, Investigation, Formal analysis, Validation, Software, Methodology, Conceptualization. **Ersilia Giordano:** Visualization, Writing – original draft, Data curation, Investigation, Formal analysis, Validation, Software, Methodology, Conceptualization. **Francesca Roscini:** Supervision, Writing – review & editing, Validation, Methodology, Conceptualization. **Francesco Clementi:** Supervision, Writing – review & editing, Validation, Methodology, Conceptualization.

Declaration of Competing Interest

The authors declare that they have no known competing financial interests or personal relationships that could have appeared to influence the work reported in this paper.

Data availability

The datasets generated during and/or analyzed during the current study are available from the corresponding author on reasonable request.

Acknowledgments

The authors express their gratitude to Itasca Harpaceas for providing access and support for 3DEC© under the IEP program as well as the Italian Ministry of University (Italy) for the support under the program "Dipartimento di Eccellenza" of the Department of Civil and Building Engineering, and Architecture—Polytechnic University of Marche (Ancona, Italy).

Fundings

The authors declare that no funds, grants, or other support were received during the preparation of this manuscript.

References

[1] Milani G. Lesson learned after the Emilia-Romagna, Italy, 20–29 May 2012 earthquakes: A limit analysis insight on three masonry churches. Eng Fail Anal 2013;34:761–78. https://doi.org/10.1016/j.engfailanal.2013.01.001.

[2] Mallardo V, Malvezzi R, Milani E, Milani G. Seismic vulnerability of historical masonry buildings: A case study in Ferrara. Eng Struct 2008;30:2223–41. https://doi.org/10.1016/j.engstruct.2007.11.006.

[3] Malena M, Angelillo M, Fortunato A, de Felice G, Mascolo I. Arch bridges subject to pier settlements: continuous vs. piecewise rigid displacement methods. Meccanica 2021;56:2487–505. https://doi.org/10.1007/s11012-021-01397-1.

[4] Malena M, de Felice G, Marfia S. AnMas: Anisotropic strength domain for masonry. Eng Struct 2022;257:114050. https://doi.org/10.1016/j.engstruct.2022.114050.

[5] García-Macías E, Ubertini F. Seismic interferometry for earthquake-induced damage identification in historic masonry towers. Mech Syst Signal Process 2019; 132:380–404. https://doi.org/10.1016/j.ymssp.2019.06.037.

[6] Cavalagli N, Comanducci G, Ubertini F. Earthquake-Induced Damage Detection in a Monumental Masonry Bell-Tower Using Long-Term Dynamic Monitoring Data. J Earthq Eng 2018;22:96–119. https://doi.org/10.1080/13632469.2017.1323048.

[7] Clementi F. Failure Analysis of Apennine Masonry Churches Severely Damaged during the 2016 Central Italy Seismic Sequence. Buildings 2021;11:58. https://doi.org/10.3390/buildings11020058.

[8] Sorrentino L, Cattari S, da Porto F, Magenes G, Penna A. Seismic behaviour of ordinary masonry buildings during the 2016 central Italy earthquakes. Bull Earthq Eng 2016;17(2019):5583–607. https://doi.org/10.1007/s10518-018-0370-4.

[9] Ferrante A, Loverdos D, Clementi F, Milani G, Formisano A, Lenci S, et al. Discontinuous approaches for nonlinear dynamic analyses of an ancient masonry tower. Eng Struct 2021;230:111626. https://doi.org/10.1016/j.engstruct.2020.111626.

[10] Formisano A, Feo PD, Grippa MR, Florio G. L'Aquila earthquake: A survey in the historical centre of Castelvecchio Subequo. COST ACTION C26: Urban Habitat Constructions under Catastrophic Events - Proceedings of the Final Conference (2010) pp. 371-376.

[11] Chieffo N, Formisano A, Miguel Ferreira T. Damage scenario-based approach and retrofitting strategies for seismic risk mitigation: an application to the historical Centre of Sant'Antimo (Italy). Eur J Environ Civ Eng 2021;25:1929–48. https://doi.org/10.1080/19648189.2019.1596164.

[12] Chieffo N, Formisano A. The Influence of Geo-Hazard Effects on the Physical Vulnerability Assessment of the Built Heritage: An Application in a District of Naples. Buildings 2019;9:26. https://doi.org/10.3390/buildings9010026.

[13] Formisano A, Chieffo N, Mosoarca M. Seismic Vulnerability and Damage Speedy Estimation of an Urban Sector within the Municipality of San Potito Sannitico (Caserta, Italy). Open Civ Eng J 2017;11:1106–21. https://doi.org/10.2174/1874149501711011106.

[14] Chieffo N, Formisano A. Geo-Hazard-Based Approach for the Estimation of Seismic Vulnerability and Damage Scenarios of the Old City of Senerchia (Avellino, Italy). Geosciences 2019;9:59. https://doi.org/10.3390/geosciences9020059.

[15] Bartoli G, Betti M, Vignoli A. A numerical study on seismic risk assessment of historic masonry towers: a case study in San Gimignano. Bull Earthq Eng 2016;14: 1475–518. https://doi.org/10.1007/s10518-016-9892-9.

[16] Bartoli G, Betti M, Vignoli A, Castellazzi G, D'Altri AM, de Miranda S, et al. Numerical insights on the seismic behavior of a non-isolated historical masonry tower. Bull Earthq Eng 2018;14:933–61. https://doi.org/10.1007/s10518-017-0231-6.

[17] Degli Abbati S, D'Altri AM, Ottonelli D, Castellazzi G, Cattari S, de Miranda S, et al. Seismic assessment of interacting structural units in complex historic masonry constructions by nonlinear static analyses. Comput Struct 2019;213:51–71. https://doi.org/10.1016/j.compstruc.2018.12.001.

[18] Magrinelli E, Acito M, Bocciarelli M. Numerical insight on the interaction effects of a confined masonry tower. Eng Struct 2021;237:112195. https://doi.org/10.1016/j.engstruct.2021.112195.

[19] Lagomarsino S, Penna A, Galasco A, Cattari S. TREMURI program: An equivalent frame model for the nonlinear seismic analysis of masonry buildings. Eng Struct 2013;56:1787–99. https://doi.org/10.1016/j.engstruct.2013.08.002.

[20] D'Altri AM, Sarhosis V, Milani G, Rots J, Cattari S, Lagomarsino S, et al. Modeling Strategies for the Computational Analysis of Unreinforced Masonry Structures: Review and Classification. Arch Comput Methods Eng 2020;27:1153–85. https://doi.org/10.1007/s11831-019-09351-x.

[21] Lemos JV. Discrete Element Modeling of Masonry Structures. Int J Archit Herit 2007;1:190–213. https://doi.org/10.1080/15583050601176868.

[22] Sandoval C, Arnau O. Experimental characterization and detailed micro-modeling of multi-perforated clay brick masonry structural response. Mater Struct 2017;50: 34. https://doi.org/10.1617/s11527-016-0888-3.

[23] Calderón S, Sandoval C, Arnau O. Shear response of partially-grouted reinforced masonry walls with a central opening: Testing and detailed micro-modelling. Mater Des 2017;118:122–37. https://doi.org/10.1016/j.matdes.2017.01.019.

[24] Ferrante A, Schiavoni M, Bianconi F, Milani G, Clementi F. Influence of Stereotomy on Discrete Approaches Applied to an Ancient Church in Muccia, Italy. J Eng Mech 2021;147:04021103. https://doi.org/10.1061/(ASCE)EM.1943-7889.0002000.

[25] Lourenço PB, Rots JG. Multisurface Interface Model for Analysis of Masonry Structures. J Eng Mech 1997;123:660–8. https://doi.org/10.1061/(ASCE)0733-9399(1997)123:7(660).

[26] Lourenço PB. Recent advances in masonry modelling: micromodelling and homogenisation. In: Multiscale Model. Solid Mech. Comput. Approaches, 2009: pp. 251–294. 10.1142/9781848163089_0006.

[27] Bagnéris M, Cherblanc F, Bromblet P, Gattet E, Gügi L, Nony N, et al. A complete methodology for the mechanical diagnosis of statue provided by innovative uses of 3D model. Application to the imperial marble statue of Alba-la-Romaine (France). J Cult Herit 2017;28:109–16. https://doi.org/10.1016/j.culher.2017.05.002.

[28] Reccia E, Cazzani A, Cecchi A. FEM-DEM Modeling for Out-of-plane Loaded Masonry Panels: A Limit Analysis Approach. Open Civ Eng J 2012;6:231–8. https://doi.org/10.2174/1874149501206010231.

[29] Giordano E, Clementi F, Nespeca A, Lenci S. Damage Assessment by Numerical Modeling of Sant'Agostino's Sanctuary in Offida During the Central Italy 2016–2017 Seismic Sequence. Front Built Environ 2019;4. https://doi.org/10.3389/fbuil.2018.00087.

[30] Facchini L, Betti M, Corazzi R, Kovacevic VC. Nonlinear seismic behavior of historical masonry towers by means of different numerical models. Procedia Eng 2017;199:601–6. https://doi.org/10.1016/j.proeng.2017.09.103.

[31] Illampas R, Ioannou I, Lourenço PB. Seismic appraisal of heritage ruins: The case study of the St. Mary of Carmel church in Cyprus. Eng Struct 2020;224:111209. https://doi.org/10.1016/j.engstruct.2020.111209.

[32] Valente M, Milani G. Seismic assessment of historical masonry structures through advanced nonlinear dynamic simulations: applications to castles, churches, and palaces, in: Numer. Model. Mason. Hist. Struct., Elsevier, 2019: pp. 163–200. 10.1016/B978-0-08-102439-3.00005-1.

[33] Clementi F, Gazzani V, Poiani M, Lenci S. Assessment of seismic behaviour of heritage masonry buildings using numerical modelling. J Build Eng 2016:29–47. https://doi.org/10.1016/j.jobe.2016.09.005.

[34] Salachoris GP, Magagnini E, Clementi F. Mechanical characterization of "Scaglia Rossa" stone masonry through experimental and numerical analyses. Constr Build Mater 2021;303:124572. https://doi.org/10.1016/j.conbuildmat.2021.124572.

[35] Valente M, Milani G. Non-linear dynamic and static analyses on eight historical masonry towers in the North-East of Italy. Eng Struct 2016;114:241–70. https://doi.org/10.1016/j.engstruct.2016.02.004.

[36] Itasca Consulting Group Inc., 3DEC- 3D Distinct Element Code, Version 7.0, User's Manual, (2013).

[37] Chetouane B, Dubois F, Vinches M, Bohatier C. NSCD discrete element method for modelling masonry structures. Int J Numer Methods Eng 2005;64:65–94. https://doi.org/10.1002/nme.1358.

[38] Dubois F, Acary V, Jean M. The Contact Dynamics method: A nonsmooth story. Comptes Rendus Mécanique 2018;346:247–62. https://doi.org/10.1016/j.crme.2017.12.009.

[39] Midas FEA NX, Analysis reference, (2020).

[40] Lee J, Fenves GL. Plastic-Damage Model for Cyclic Loading of Concrete Structures. J Eng Mech 1998;124:892–900. https://doi.org/10.1061/(ASCE)0733-9399(1998)124:8(892).

[41] Valente M, Milani G. Effects of Geometrical Features on the Seismic Response of Historical Masonry Towers. J Earthq Eng 2018;22:2–34. https://doi.org/10.1080/13632469.2016.1277438.

[42] Milani G, Valente M. Failure analysis of seven masonry churches severely damaged during the 2012 Emilia-Romagna (Italy) earthquake: Non-linear dynamic analyses vs conventional static approaches. Eng Fail Anal 2012;54(2015):13–56. https://doi.org/10.1016/j.engfailanal.2015.03.016.

[43] Castellazzi G, D'Altri AM, de Miranda S, Ubertini F. An innovative numerical modeling strategy for the structural analysis of historical monumental buildings. Eng Struct 2017;132:229–48. https://doi.org/10.1016/j.engstruct.2016.11.032.

[44] Castellazzi G, D'Altri AM, de Miranda S, Chiozzi A, Tralli A. Numerical insights on the seismic behavior of a non-isolated historical masonry tower. Bull Earthq Eng 2018;16:933–61. https://doi.org/10.1007/s10518-017-0231-6.

[45] Lubliner J, Oliver J, Oller S, Oñate E. A plastic-damage model for concrete. Int J Solids Struct 1989;25:299–326. https://doi.org/10.1016/0020-7683(89)90050-4.

[46] Ministero delle Infrastrutture e dei Trasporti, Aggiornamento delle "Norme Tecniche per le Costruzioni" - NTC 2018 (in italian), (2018) 1–198.

[47] Ministero delle infrastrutture e dei trasporti, Circolare 21 gennaio 2019 n. 7 C.S.LL. PP. Istruzioni per l'applicazione dell'aggiornamento delle "Norme Tecniche per le

Costruzioni" di cui al D.M. 17/01/2018 (in Italian), Suppl. Ord. Alla G.U. n. 35 Del 11/2/19. (2019).
[48] Vasconcelos G, Lourenço PB. Experimental characterization of stone masonry in shear and compression. Constr Build Mater 2009;23:3337–45. https://doi.org/10.1016/j.conbuildmat.2009.06.045.
[49] Ferrante A, Clementi F, Milani G. Dynamic behavior of an inclined existing masonry tower in Italy. Front. Built Environ 2019;5:1–16. https://doi.org/10.3389/fbuil.2019.00033.
[50] Ferrante A, Clementi F, Milani G. Advanced numerical analyses by the Non-Smooth Contact Dynamics method of an ancient masonry bell tower. Math Methods Appl Sci 2020:mma.6113. https://doi.org/10.1002/mma.6113.
[51] INGV, Istituto Nazionale di Geofisica e Vulcanologia, (2020).